Research Article Vol. 56, No. 21 / July 20 2017 / Applied Optics 5857

applied optics

# Correcting groove error in gratings ruled on a 500-mm ruling engine using interferometric control

Xiaotao Mi,[1,2,*] Haili Yu,[1] Hongzhu Yu,[1] Shanwen Zhang,[1] Xiaotian Li,[1] Xuefeng Yao,[1] Xiangdong Qi,[1] Bayinhedhig,[1] and Qiuhua Wan[1]

[1]Grating Technology Laboratory, Changchun Institute of Optics and Fine Mechanics and Physics, Chinese Academy of Sciences, Changchun, Jilin 130033, China
[2]University of Chinese Academy of Sciences, Beijing 100049, China
*Corresponding author: mixiaotao_ciomp@126.com

Received 27 April 2017; revised 19 June 2017; accepted 22 June 2017; posted 22 June 2017 (Doc. ID 294616); published 13 July 2017

**Groove error is one of the most important factors affecting grating quality and spectral performance. To reduce groove error, we propose a new ruling-tool carriage system based on aerostatic guideways. We design a new blank carriage system with double piezoelectric actuators. We also propose a completely closed-loop servo-control system with a new optical measurement system that can control the position of the diamond relative to the blank. To evaluate our proposed methods, we produced several gratings, including an echelle grating with 79 grooves/mm, a grating with 768 grooves/mm, and a high-density grating with 6000 grooves/mm. The results show that our methods effectively reduce groove error in ruled gratings.** 

***OCIS codes:*** (050.1950) Diffraction gratings; (050.0050) Diffraction and gratings; (120.0120) Instrumentation, measurement, and metrology; (120.4640) Optical instruments.

https://doi.org/10.1364/AO.56.005857

## 1. INTRODUCTION

The simplicity and speed of grating spectroscopy, and its advantages in the polarization and phase matching, have led to an urgent demand for gratings and echelles, especially those of high quality with large sizes in fields such as astronomy, military, aerospace, and biochemical analysis [1–5]. The mechanical ruling method, one of the most important ways to produce gratings, is mainly used to produce echelle gratings and infrared-laser gratings that have deep grooves with strict shapes [4,6].

When gratings are ruled, a variety of errors can be produced, including straightness errors in blank carriageways and aerostatic guideways, or cumulative and periodic screw errors. Such errors can lead to groove error in ruled gratings, so the gratings are inferior in quality [7,8]. Therefore, many scholars have studied how to correct the groove error of gratings using reasonable mechanical structures and interferometric control [9–17].

The current largest ruling engine in the world is the MIT-C engine, which has the ability to rule blanks of sizes up to 450 mm × 650 mm × 125 mm. A continuous-motion system of interferometric control is adopted for the MIT-C engine. The diamond carriage system of MIT-C is an open loop-control system, so the groove error is determined by the mechanical structure. The diamond carriage system includes a cylindrical monorail, a slide bearing, and a fused-silica guide. The fused-silica guide is 100 mm × 100 mm × 510 mm, and its guide plane is worked straight to within a quarter fringe. The diamond carriage hangs from the slide bearing riding on the cylindrical monorail and presses against the guide plane via a Rulon-covered button. The blank carriage system is a closed-loop system; the groove error of the system is measured by the interferometer, and a servo motor is used to correct the error in real time. Well-blazed and high-quality gratings have been produced by MIT-C at spacing between 31.6 and 632 grooves/mm [18–20].

In the present paper, we propose several methods to correct the groove error of CIOMP-6 in China, which can rule blanks of up to 400 mm × 500 mm × 100 mm. To reduce the groove error, we propose a new ruling-tool carriage system based on aerostatic guideways and design a new blank carriage system with double piezoelectric actuators. We also propose a completely closed-loop servo-control system with an optical measurement system that can control the position of the diamond relative to the blank. We used an interferometer as a measuring and feedback component and designed a control system with macro and micro positioning. When the groove error of the gratings is measured by the interferometer, the proposed control system corrects the groove error in real time.

## 2. THEORY

The groove error is the error between the ideal groove and actual groove, as shown in Fig. 1. The groove error matrix can be written as

$$\boldsymbol{\delta}_{nm} = \begin{bmatrix} \delta_{11} & \delta_{21} & \cdots & \delta_{n1} \\ \delta_{12} & \delta_{22} & \cdots & \delta_{n2} \\ \vdots & \vdots & \vdots & \vdots \\ \delta_{1m} & \delta_{2m} & \cdots & \delta_{nm} \end{bmatrix}, \tag{1}$$

where the rows represent the ruling grooves, and the columns represent different positions on the grooves.

The optical path difference caused by groove error can be given as

$$\eta = \delta_{nm} \times (\sin\theta_i + \sin\theta_d), \tag{2}$$

where $\theta_i$ is the incidence angle, and $\theta_d$ is the diffraction angle.

The grating diffraction equation is as follows:

$$d \times (\sin\theta_i + \sin\theta_d) = m\lambda, \tag{3}$$

where $d$ is grating constant, $m$ is grating diffraction order, and $\lambda$ is incidence wavelength.

By combining Eqs. (1), (2), and (3), the diffraction wavefront of grating can be written as

$$\Delta(m) = \frac{m\lambda}{d}\begin{bmatrix} \delta_{11} & \delta_{21} & \cdots & \delta_{n1} \\ \delta_{12} & \delta_{22} & \cdots & \delta_{n2} \\ \vdots & \vdots & \vdots & \vdots \\ \delta_{1m} & \delta_{2m} & \cdots & \delta_{nm} \end{bmatrix}. \tag{4}$$

Any random errors in groove error $\delta_{nm}$ will generate scattered light between the spectral orders. Under the Littrow configuration, the proportion of incident light thus scattered is given by

$$\frac{I_{st}}{I_i} = \left(\frac{2\pi m\delta_{\text{rms}}}{d}\right)^2, \tag{5}$$

where $I_{st}$ is the sum of all the scattered light intensities of the spectral image plane, $I_i$ is the intensity of the incident light, and $\delta_{\text{rms}}$ is the root-mean-square (RMS) error of $\delta_{nm}$.

If there are periodic errors in $\delta_{nm}$, then these will generate ghosts. In the Littrow configuration, the intensity of ghosts relative to the main diffracted order is given by

$$\frac{I_g}{I_d} = \left[J_n\left(\frac{2\pi m\varepsilon}{d}\right)\right]^2, \tag{6}$$

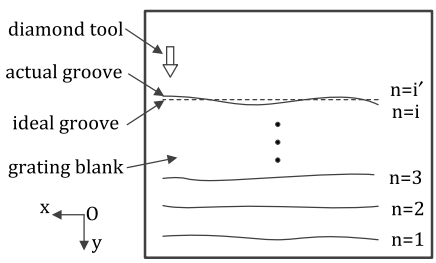


**Fig. 1.** Groove error when grating is ruled.

**Table 1. Values of $\delta_{\text{pv}}$, $\delta_{\text{rms}}$, and $\varepsilon$ of Groove Error**

| Groove density | Blazed order | $\delta_{\text{pv}}$ (nm) | $\delta_{\text{rms}}$ (nm) | $\varepsilon$ (nm) |
|---|---|---|---|---|
| 768 | 1 | 325.52 | 20.72 | 0.207 |
| 79 | −36 | 87.90 | 5.60 | 0.056 |
| 6000 | 1 | 41.67 | 2.65 | 0.026 |

where $I_g$ is the intensity of ghosts, $I_d$ is the intensity of main diffracted order, $J_n$ is n-order Bessel function, and ε is the harmonic amplitude of the periodic error of $\delta_{nm}$.

As can be observed from Eqs. (4)–(6), the groove error increases with increasing diffraction order and grating density. From the spectroscopic point of view, we expect the wavefront of the gratings to be better than $0.25\lambda$ ($\lambda = 632.8$ nm). A value of 1% of scattered light ($I_{st}/I_i$) will be a reasonable figure, and we accept a figure of $10^{-6}$ or lower for ghosts ($I_g/I_d$) as being realistic. Then, the values of $\delta_{\text{pv}}$ (where $\delta_{\text{pv}} = \delta_{\text{peak}} - \delta_{\text{valley}}$), $\delta_{\text{rms}}$, and ε are calculated and listed in Table 1.

As shown in Table 1, the echelles or gratings with high grating density require little groove error, so both reasonable mechanical structure and interferometric control must be used to correct groove errors that occur on the ruling engine.

## 3. CIOMP-6 RULING ENGINE

### A. Description of CIOMP-6

The CIOMP-6 ruling engine was developed by the Changchun Institute of Optics and Fine Mechanics and Physics (CIOMP). Like CIOMP-2 [12], CIOMP-6 uses stop-start blank advance, which helps reduce internal vibrations and makes practicable an interferometric closed-loop servo-control system that we believe to be primarily responsible for the success of the engine. To ensure the quality of the gratings does not change in different areas, large gratings require a more reasonable mechanical structure and more precise controls than smaller gratings.

CIOMP-6 is shown in Fig. 2. A new ruling-tool carriage system based on aerostatic guideways is proposed, and a new blank carriage system with double piezoelectric actuators is designed. A completely closed-loop servo-control system with a new optical measurement system that can control the position of diamond relative to the blank is also proposed. Usually, the temperature is controlled in various stages; the temperature in the core area of the engine can be controlled to within 0.01°C.

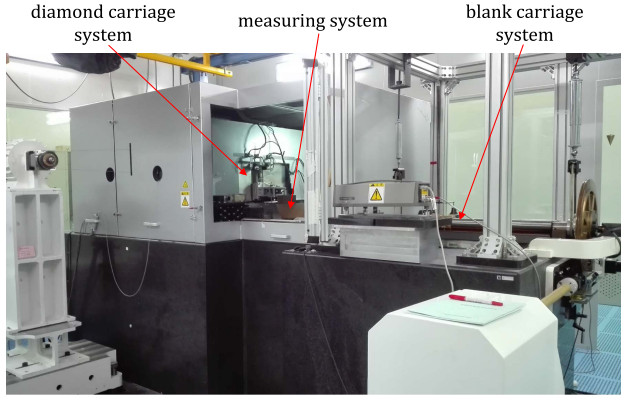


**Fig. 2.** CIOMP-6 grating ruling engine.

The 2407-kg ruling engine is mounted on a 7950-kg slab of reinforced concrete held on 12 air suspension cylinders set with a resonance frequency of 1 Hz.

### B. Diamond Carriage System

During the course of ruling a grating, the diamond travels long distances at high speeds. Therefore, the materials of the guideways, which are susceptible to the effects of wear, must be chosen with great care. The fundamental mechanical difference between CIOMP-6 and other engines lies in the method used to reduce wear between the diamond carriage and its guideways. In the MIT-B and MIT-C ruling engines, the weight of the diamond carriage is borne by a cylindrical monorail. The engine guide is provided by a Rulon shoe in contact with a glass optical flat. Wear mainly occurs at the cylindrical monorail. In contrast, in the CIOMP-2 engine, the saddle slider rides directly on a glass guideway; therefore, wear between shoes and the guideway is inevitable. In the CIOMP-6 engine, we chose aerostatic guideways for the diamond carriage. The static guide is granite, which has the advantages of a small coefficient of linear expansion and excellent thermal stability. The slider uses an aluminum alloy that has the advantages of being lightweight and having excellent dynamic performance (see Fig. 3). In addition, unlike other machines, we choose a flexible wire rope to drive the slider that can effectively reduce the vibration caused by the push–pull rod.

The tool holder consists of two cross-hinge steel springs, and the weight is used to control the groove depth (see Fig. 4). Considering the convenience of disassembly and assembly of the tool holder, the diamond carriage with the tool holder is mounted on the side of the slider. To prevent sideways movement of the diamond tip, the adjustable balance weight block is fixed on the other side of the slider. The two sets of aerostatic guideways are arranged in parallel to improve the rigidity of the guideways. The driving force acts on the center of the guideways to avoid the introduction of lateral forces. In the new driving structure of the diamond carriage, motor $A$ induces a reciprocating action of the diamond carriage via the wire rope and pulley group (see Fig. 3).

In the new ruling system, the straightness error of the aerostatic guideways and the deflection error of the moving slider relative to the static guide are the main factors that cause groove error. The straightness error of the aerostatic guideways is found to be 0.05 arcsec in 420 mm of translation when uncorrected; this varies even with small temperature and pressure fluctuations. From the geometric relationship in Fig. 5, the deflection error can be given by

$$\delta_1 = \delta_h + \delta_l = h \sin\theta + l(1 - \cos\theta). \tag{7}$$

The deflection error varies with the position of the slider in the static guide and with small pressure fluctuations. Although the structure of the aerostatic guideways effectively reduces the deflection, the effect of deflection error on the groove error cannot be neglected. The $\delta_{pv}$ in the single 400-mm-long groove caused by the straightness error of aerostatic guideways and the deflection error of the moving slider relative to the static guide; the value of $\delta_{pv}$ is found to be more than 200 nm, that cannot meet the requirements in Table 1.

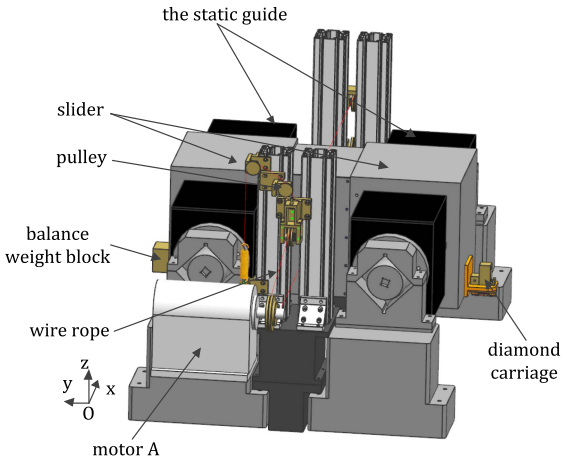


**Fig. 3.** New mechanical structure of the diamond carriage system.

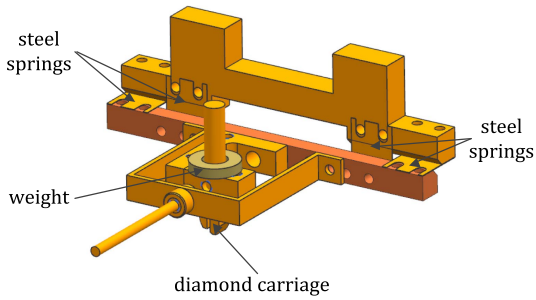


**Fig. 4.** Structure of the tool holder.

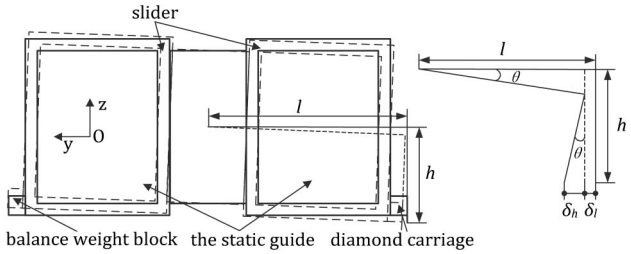


**Fig. 5.** Influence of the deflection error of the moving slider relative to the static guide on the groove error.

### C. Blank Carriage System

As with most ruling engines, the blank carriage system moves slowly along the direction orthogonal to the ruling system. As shown in Fig. 6, the rotational movement of the motor $B$ is converted into linear motion via a set of gears, worm–gear pairs, and leadscrew nut vices. If there is no error correction in 700 mm of travel, periodic errors and cumulative errors of the transmission mechanism are 200 nm and 5 μm, respectively, and the yaw error of the blank carriage is 0.2 arcsec. We can see that the mechanical tolerances imposed upon the blank carriage system are severe and impractical for ruling high-quality gratings.

Combining the advantages of the MIT-C engine and our successful experience with the CIOMP-2 engine, we designed a new structure for the blank carriage with double piezoelectric

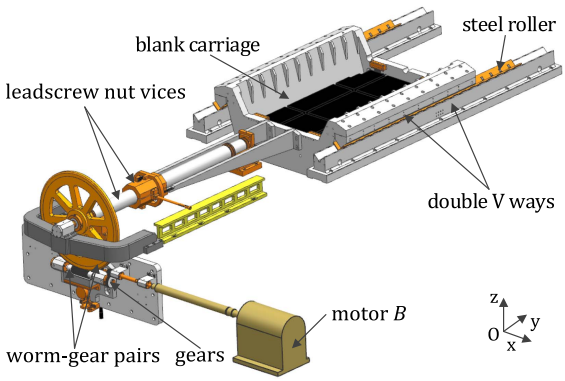


**Fig. 6.** Mechanical structure of the blank carriage.

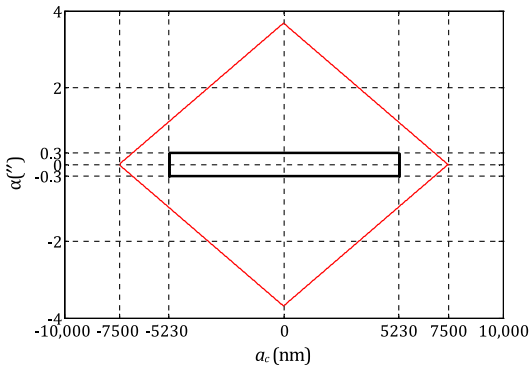


**Fig. 8.** Ability of the new blank carriage to correct the groove error.

actuators to correct the groove error of the ruling engine. Like the MIT-C engine, the blank carriage slides on steel rollers between double V ways. Using double V ways with 80 steel rollers spaced 60 mm apart removes the limitation on grating weight. This also reduces friction between the heavy blank carriage and the V ways. The blank is mounted on the inner carriage. The inner carriage is suspended in the outer carriage using four parallel leaf springs, as in the CIOMP-2 engine. The double piezoelectric actuators are fixed between the inner carriage and the outer carriage. Two extension springs are used to keep the double piezoelectric actuators in close contact with the inner carriage. When a grating is being ruled, the length of the double actuators is varied without friction to correct groove errors and keep the inner carriage in the predetermined position (see Fig. 7).

The maximum elongation of the piezoelectric actuator is 15 μm; half of this elongation length is set to the zero position. When the gratings begin to rule, the piezoelectric actuator is in the zero position. From the geometric relationship of blank carriage in Fig. 7, the ability of the new blank carriage to correct groove errors can be written as

$$\begin{cases} \alpha = \arctan\left(\frac{a_1 - a_2}{a}\right) \\ a_c = \frac{a_1 + a_2}{2} \end{cases}, \quad -7.5 \le a_1 \le 7.5\ \mu\text{m}, -7.5 \le a_2 \le 7.5\ \mu\text{m}, \tag{8}$$

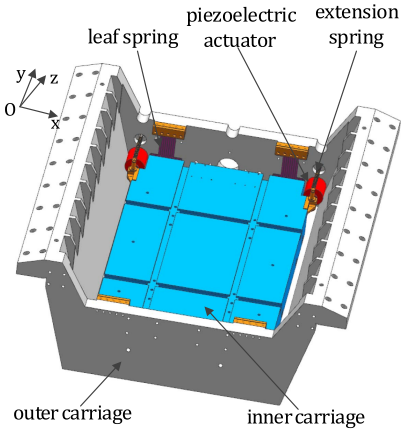


**Fig. 7.** New mechanical structure of the blank carriage.

where $\alpha$ is the correction ability of angle errors, $a_c$ is the correction ability of displacement errors, $a_1$ and $a_2$ are the displacement of the double piezoelectric actuators, and $a$ (420 mm) is the distance between the piezoelectric actuator axes.

The error of each groove can be divided into angle error and displacement errors. The angle error is mainly caused by the yaw error of the blank carriage and the straightness of aerostatic guide ways. The displacement error mainly includes errors of the transmission mechanism and the Abbe error of the new measuring system, which will be discussed in the following section. If a 400 mm × 500 mm × 100 mm grating is ruled without groove error correction, the maximum values of the angle error and the displacement error are calculated to be about 0.3 arcsec and 5.23 μm, respectively.

In the meantime, the ability of the new blank carriage to correct the groove error and the possible values of the groove error that need to be corrected can be intuitively expressed, as shown in Fig. 8.

As shown in Fig. 8, the rhombus-shaped area and the rectangular area represent the correction ability of the new blank carriage and the possible values of the groove error, respectively. Accordingly, the correction ability of the new blank carriage can meet the required of groove error corrections. In addition, many ruling experiments and simulation ruling experiments have revealed that the CIOMP-6 engine has the ability to rule a 400 mm × 500 mm × 100 mm grating.

### D. Measurement System

To measure the groove error of the ruling engine, including the diamond carriage system and the blank carriage system, we mounted an interferometer and a reference mirror on the diamond carriage and put the measuring mirror on the inner carriage. The pitch error of the carriage during the 700-mm traverse was found to be 0.2 arcsec. The Abbe error caused by the pitch error of the carriage and the deflection error of the moving slider relative to the static guide must be corrected, as the ruling plane and the measuring plan are separated by several tens of millimeters. As shown in Fig. 9, the Abbe error can be given by

$$\delta_2 = \delta_m - \delta_r = h_1 \times \tan\beta, \tag{9}$$

where $\delta_2$ is the Abbe error, $\delta_m$ is the measured groove error, $\delta_r$ is the actual groove error, $h_1$ is the distance between the ruling

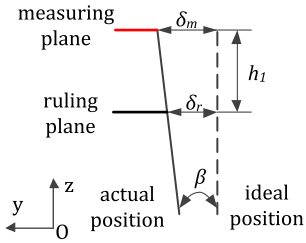


**Fig. 9.** Schematic diagram of Abbe error.

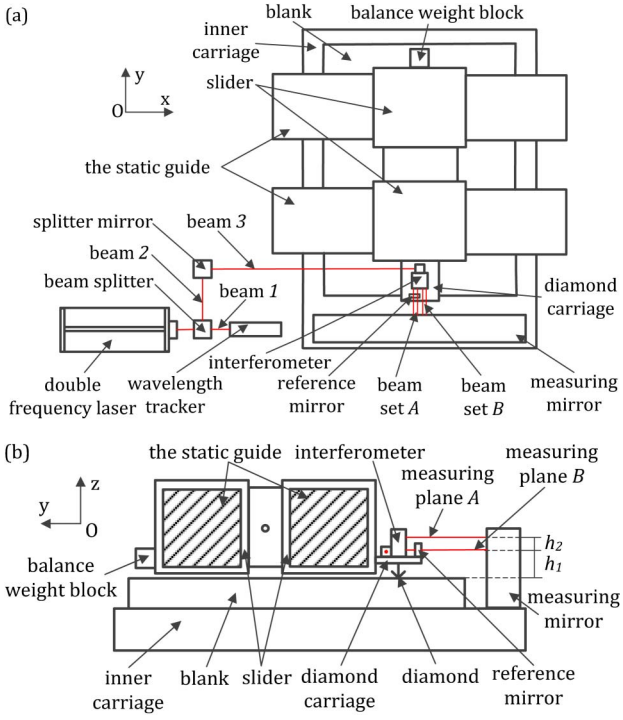


**Fig. 10.** New optical measurement system: (a) top view; (b) side view.

plane and the measuring plane, and $\beta$ is the sum of the pitch error of the carriage and the deflection error of the moving slider relative to the static guide.

Considering the Abbe error measurement, we designed a new optical measurement system shown in Fig. 10.

Figure 10 shows a schematic of the new optical measurement system. A laser beam with $\lambda = 632.8$ nm is split into two beams by a beam splitter. Beam 1 incidents into a wavelength tracker to compensate for errors that are caused by changes in the refractive index of the air. Beam 2 passes into the interferometer via a splitter mirror and is then split into two sets of beams. Beam set $A$ is used to measure the displacement between the reference mirror and the measuring mirror; beam set $B$ is used to measure the Abbe error.

As shown in Figs. 10 and 11, to measure Abbe error, two measuring planes are designed in the new optical measurement system. The beams of beam set $A$ in measuring plane $A$ are incident on the measuring mirror, and those of beam set $A$ in measuring plane $B$ are incident on the reference mirror.

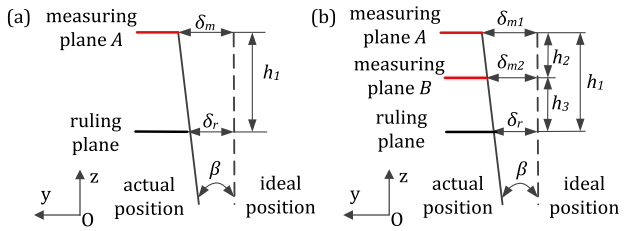


**Fig. 11.** Schematic diagram of the optical measurement system of Abbe error: (a) beam set $A$; (b) beam set $B$.

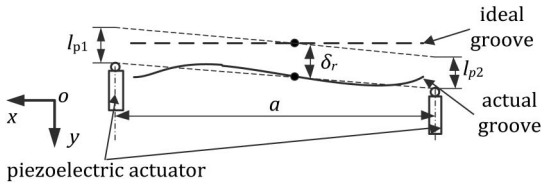


**Fig. 12.** Schematic of the double piezoelectric actuators achieved for groove error correction.

All the beams in beam set $B$ are incident on the measuring mirror in the two measuring planes. According to Figs. 10 and 11, the groove error in the ruling plane is given as

$$\delta_r = \delta_m - h_1 \times \tan\beta = \delta_m - h_1 \times \frac{\delta_{m1} - \delta_{m2}}{h_2}, \tag{10}$$

where $\delta_{m1}$ is the measured groove error in measuring plane $A$, $\delta_{m2}$ is the measured groove error in measuring plane $B$, and $h_2$ is the distance between measuring plane $A$ and measuring plane $B$.

### E. Principle of Groove Error Correction

For the diamond carriage system, we need to measure the position of the slider through a grating ruler to control the direction of motor $A$ and the diamond lifter. The groove error is corrected by the blank carriage system using macro positioning and micro positioning. In macro positioning, motor $B$ drives blanks to move at a grating constant. This will cause groove errors due to the mechanical and measuring system.

These groove errors can be measured by the new optical measurement system. The micro positioning system then adjusts the lengths of the double piezoelectric actuators, $l_{p1}$ and $l_{p2}$, to keep the groove in the ideal position in real time. As shown in Fig. 12, the length of the double piezoelectric actuators is given by

$$l_{p1} = l_{p2} = \delta_r. \tag{11}$$

### F. Limitations on Ruling Speed

A 500-mm-wide grating requires 7 to 15 days for ruling on the CIOMP-6 engine. The speed of grating ruling is limited to 6 grooves/ min by internal vibrations. For the new ruling-tool carriage system based on aerostatic guideways, diamond speed is not the major factor limiting the speed of ruling. Rather, it is limited by the rate of blank motion. Many experiments have revealed that the intensity of scattered light increases with increasing speed of the blank under the same grating density.

Under ideal conditions, the outer carriage remains still when the gratings are being ruled. In practice, the outer carriage with the blank continues to move because of inertia, while the piezoelectric actuators are correcting for groove errors. This causes internal vibrations that increase the intensity of scattered light. When other conditions remain unchanged, reducing the ruling speed can improve the quality of the grating.

## 4. RULING EXPERIMENT

The CIOMP-6 ruling engine can now rule blanks of up to 400 mm × 500 mm, with grating densities between 30 and 6000 grooves/mm. Several high-quality gratings have been ruled by Ciomp-6. In this section we introduce the comparative experiment and three typical gratings.

### A. Comparative Experiment

To demonstrate the capability of groove error correction of CIOMP-6, two comparison experiments were carried out. In each group of the experiments, we ruled two gratings that had one with the correction of groove error and the other without groove error correction.

In the first group of comparison experiments, two echelle gratings with 79 grooves/mm were ruled. The areas of the two echelle gratings were the same, at 80 mm × 90 mm × 16 mm. The ghosts and scattered light of the echelle gratings without correction formed a bright line between the diffractive orders. The maximum intensity of the ghosts and scattered light is stronger than $10^{-3}$, and the diffraction efficiency is less than 30% at $\lambda = 632.8$ nm in the −36th order. For the gratings with groove error correction, the ghosts are weaker than $10^{-5}$, the strongest intensity of scattered light is below $10^{-4}$, and the diffraction efficiency is about 50% at $\lambda = 632.8$ nm in the −36th order. As shown in Fig. 13, the value of the wavefront decreased from $0.456\lambda$ to $0.108\lambda$ ($\lambda = 632.8$ nm) after groove error correction.

In the second comparison experiment, two 40 mm × 25 mm × 16 mm gratings with 600 grooves/mm were ruled. The scattered light of the gratings without groove error correction formed a line between the diffractive orders and ghosts. The maximum intensity of the ghosts approaches $10^{-3}$, and the diffraction efficiency is less than 70% at $\lambda = 632.8$ nm in the −1st order. For the grating with groove error correction, no ghosts are observed, the strongest intensity of scattered light

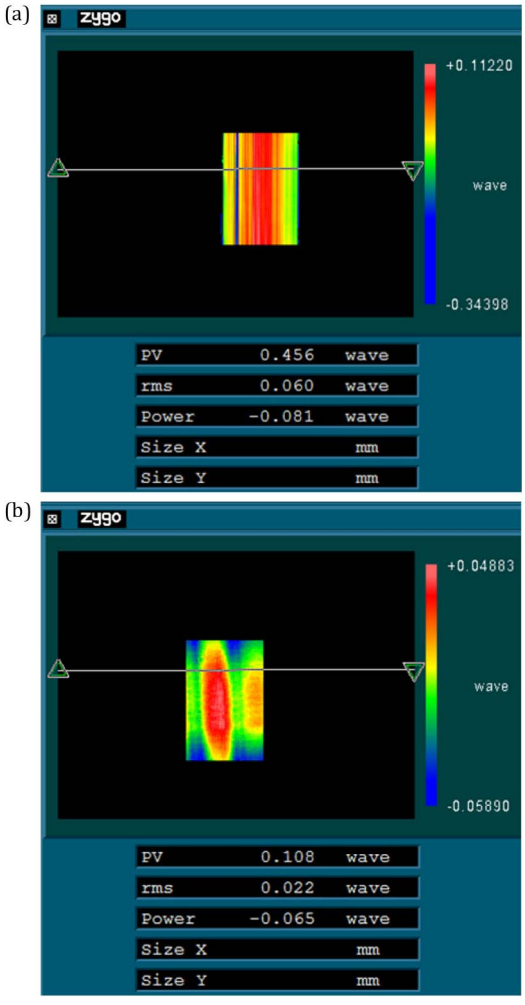


**Fig. 13.** Wavefront quality of the echelle gratings with 79 grooves/mm for comparative experiment measured by Zygo interferometer: (a) without groove error correction; (b) with groove error correction.

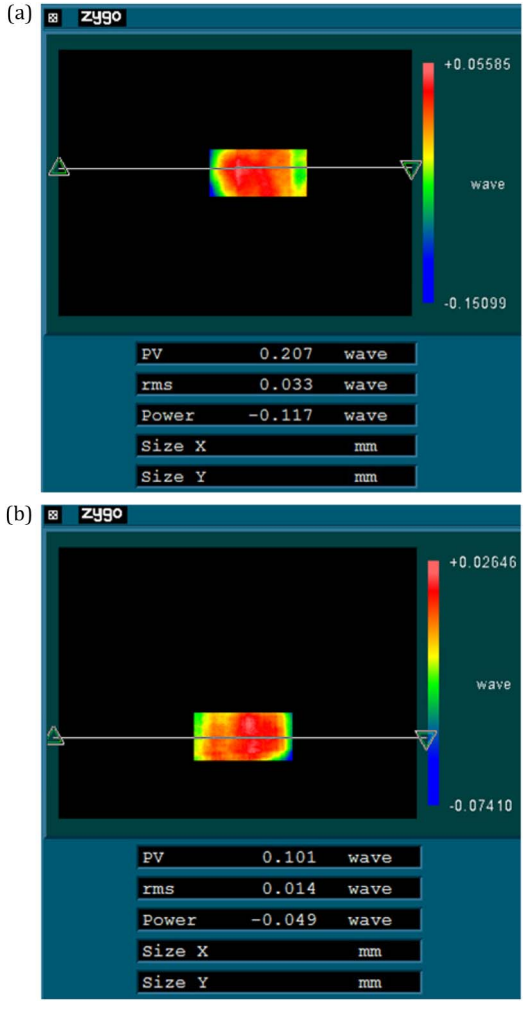


**Fig. 14.** Wavefront quality of the gratings with 600 grooves/mm for comparative experiment measured by Zygo interferometer: (a) without groove error correction; (b) with groove error correction.

reaches $10^{-5}$, and the diffraction efficiency is more than 80% at $\lambda = 632.8$ nm in −1st order. As shown in Fig. 14, the value of the wavefront decreased from $0.207\lambda$ to $0.101\lambda$ ($\lambda = 632.8$ nm) after groove error correction.

### B. Gratings Ruled ON the CIOMP-6 Engine

An echelle grating 6-79-005 with 79 grooves/mm was ruled on 80 mm × 120 mm × 16 mm rectangular blanks, blazed at 64°. No Rowland and Lyman ghosts were observed in the −1st to −36th orders. The intensity of scattered light is no stronger than $10^{-4}$. We calculated the theoretical grating efficiency of the blazed wavelength (632.8 nm) to be approximately 52.6%, and the actual efficiency was measured to be 50.3%. The grating wavefront can be measured by Zygo interferometer, as shown in Fig. 15. The figure shows that the wavefront value of diffractive order is $0.160\lambda$ ($\lambda = 632.8$ nm). The quality of echelle grating 6-79-005 is as high as echelle grating ruled by the MIT-B and MIT-C engines. Echelle grating 6-79-005 was compared with grating 5-79-003, which was ruled on the CIOMP-2 engine. The wavefront qualities of the two gratings are similar. The ghosts of echelle grating 5-79-003 approach $10^{-3}$ in intensity, and the maximum intensity of scattered light is stronger than $10^{-4}$.

6-768-001 is a 55 mm × 30 mm × 16 mm grating with 768 grooves/mm, blazed at 9°. The maximum intensity of the ghosts and scattered light can reach $10^{-5}$. For the application band from 340 nm to 540 nm, the curves of theoretical efficiency and test efficiency are shown in Fig. 16. The test value and the theoretical value are close to each other. As shown in Fig. 17, the wavefront value is $0.112\lambda$ ($\lambda = 632.8$ nm).

We tried to rule a high-groove-density grating (6-6000-1) with 6000 grooves/mm using CIOMP-6. 6-6000-1 is a 40 mm × 10 mm × 16 mm grating. As the far ultraviolet radiation is strongly absorbed by air, it is difficult to measure the efficiency, ghosts, scattered light, and wavefront of gratings blazed at such wavelengths. To evaluate the quality of the grating, the grooves were measured by an atomic force microscope. As shown in Fig. 18, the repeatability of the grooves is

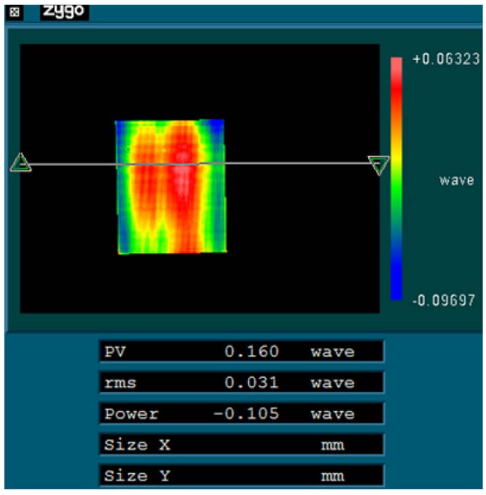


**Fig. 15.** Wavefront quality of the echelle grating 6-79-005 measured by Zygo interferometer.

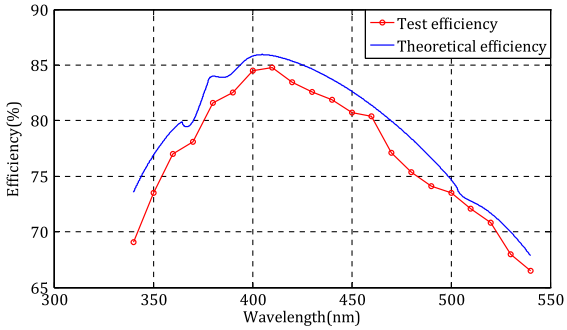


**Fig. 16.** Test efficiency and theoretical efficiency of the grating 6-768-001.

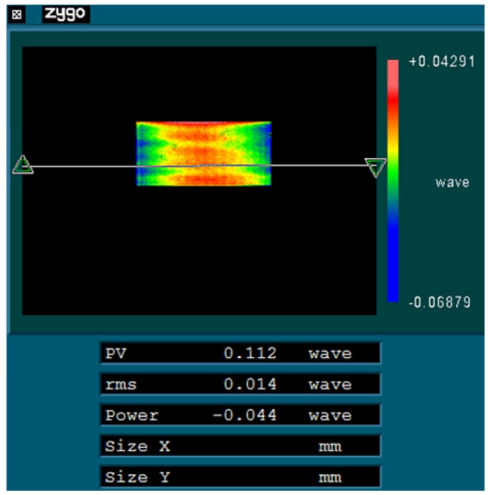


**Fig. 17.** Wavefront quality of the grating 6-768-001 measured by Zygo interferometer.

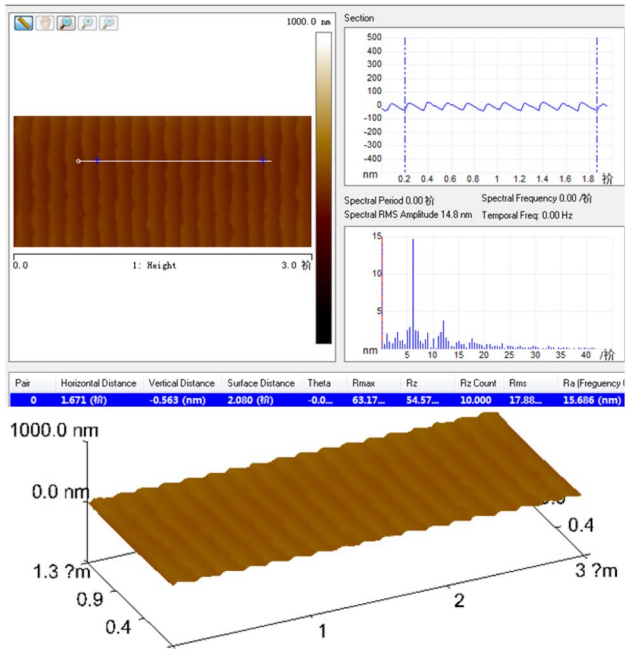


**Fig. 18.** Test results of atomic force microscope for grooves of grating 6-6000-1.

excellent, the spacing of 10 grooves is 1671 nm, and the groove error for 10 grooves is about 4 nm.

## 5. CONCLUSIONS

Groove error directly affects the quality of ruling gratings. We established a mathematical model for groove error and grating performance, including wavefront, ghosts, and scattered light. Based on this model, we showed that the echelles or gratings with high grating density require little groove error; thus, we proposed methods to correct groove errors that may be due to the ruling engine. We proposed a new ruling-tool carriage system based on aerostatic guideways and designed a new blank carriage system with double piezoelectric actuators. We also proposed a completely closed-loop servo-control system with a new optical measurement system to control the position of the diamond relative to the blank. We introduce the comparative experiments and three typical gratings. Our results showed that ghosts and scattered light reduced in intensity by 1–2 orders of magnitude through the correction of groove error. The performances of the ruled 79-groove/mm echelle grating and the 768-groove/mm grating were close to the theoretical level. The repeatability and positioning accuracy for the 6000-groove/mm grating were excellent. In conclusion, our proposed methods can effectively correct for groove errors and substantially improve grating quality.

**Funding.** Ministry of Science and Technology of the People's Republic of China (MOST) (2016YFF0102006, 2016YFF0103304); National Basic Research Program of China (2014CB049500); National Natural Science Foundation of China (NSFC) (61505204, 61605204); Jilin Province Outstanding Youth Project in China (20170520167JH).

## REFERENCES

1. R. Kammel, R. Ackermann, J. Thomas, J. Götte, S. Skupin, A. Tunnermann, and S. Nolte, "Enhancing precision in fs-laser material processing by simultaneous spatial, and temporal focusing," Light **3**, e169–8 (2014).
2. T. Jitsuno, S. Motokoshi, T. Okamoto, T. Mikami, D. Smith, M. L. Schattenburg, H. Kitamura, H. Matsuo, T. Kawasaki, K. Kondo, H. Shiraga, Y. Nakata, H. Habara, K. Tsubakimoto, R. Kodama, K. A. Tanaka, N. Miyanaga, and K. Mima, "Development of 91 cm size gratings and mirrors for LEFX laser system," J. Phys. **112**, 032002 (2008).
3. C.-H. Chang, Y. Zhao, R. K. Heilmann, and M. L. Schattenburg, "Fabrication of 50 nm period gratings with multilevel interference lithography," Opt. Lett. **33**, 1572–1573 (2008).
4. D. Nevejans, E. Neefs, E. Van Ransbeeck, S. Berkenbosch, R. Clairquin, L. De Vos, W. Moelans, S. Glorieux, A. Baeke, O. Korablev, I. Vinogradov, Y. Kalinnikov, B. Bach, J.-P. Dubois, and E. Villard, "Compact high-resolution spaceborne echelle grating spectrometer with acousto-optical tunable filter based order sorting for the infrared domain from 2.2 to 4.3 μm," Appl. Opt. **45**, 5191–5206 (2006).
5. T. Suzuki, H. Kubo, T. Suganuma, T. Yamashita, O. Wakabayashi, and H. Mizoguchi, "High-resolution multigrating spectrometer for high quality deep UV light source production," Proc. SPIE **4346**, 1254–1261 (2001).
6. I. R. Bartlett and P. C. Wildy, "Diffraction grating ruling engine with piezoelectric drive," Appl. Opt. **14**, 1–3 (1975).
7. G. R. Harrison, N. Sturgis, S. P. Davis, and Y. Yamada, "Interferometrically controlled ruling of ten-inch diffraction gratings," J. Opt. Soc. Am. **49**, 205–211 (1959).
8. G. J. Dunning and M. L. Minden, "Scattering from high efficiency diffraction gratings," Appl. Opt. **19**, 2419–2425 (1980).
9. E. Leibhardt, "Improved method for lapping a dividing gear for a ruling engine," J. Opt. Soc. Am. **42**, 447–450 (1952).
10. H. W. Babcock, "Control of a ruling engine by a modulated interferometer," Appl. Opt. **1**, 415–420 (1962).
11. C. Yang, X. T. Li, H. L. Yu, H. Z. Yu, J. W. Zhu, S. W. Zhang, J. X. Gao, Bayinheshig, and Y. G. Tang, "Practical method study on correcting yaw error of 500 mm grating blank carriage in real time," Appl. Opt. **54**, 4084–4088 (2015).
12. X. T. Li, H. L. Yu, X. D. Qi, S. L. Feng, J. C. Chu, S. W. Zhang, Jirigalantu, and Y. G. Tang, "300 mm ruling engine producing gratings and echelles under interferometric control in China," Appl. Opt. **54**, 1819–1826 (2015).
13. H. L. Yu, X. T. Li, J. W. Zhu, H. Z. Yu, X. D. Qi, and S. L. Feng, "Reducing the line curvature error of mechanically ruled gratings by interferometric control," Appl. Phys. B **117**, 279–286 (2014).
14. C. Yang, H. L. Yu, X. T. Li, J. W. Zhu, H. Z. Yu, Bayinheshig, X. D. Qi, and Y. G. Tang, "Real-time monitoring of ruling grating resolution by digital wavefront," Appl. Opt. **54**, 492–497 (2015).
15. Jirigalantu, X. T. Li, S. W. Zhang, X. T. Mi, J. X. Gao, Bayanheshig, X. D. Qi, and Y. G. Tang, "Ruling of echelles and gratings with a diamond tool by the torque equilibrium method," Appl. Opt. **55**, 8082–8088 (2016).
16. S. W. Zhang, X. T. Mi, Q. Zhang, Jirigalantu, S. L. Feng, H. L. Yu, and X. D. Qi, "Groove shape characteristics of echelle gratings with high diffraction efficiency," Opt. Commun. **387**, 401–404 (2017).
17. M. V. Zorina, S. Y. Zuev, M. S. Mikhailenko, A. E. Pestov, V. N. Polkovnikov, N. N. Salashchenko, and N. I. Chkhalo, "The diffraction efficiency of echelle gratings increased by ion-beam polishing of groove surfaces," Tech. Phys. Lett. **42**, 844–847 (2016).
18. G. R. Harrison, S. W. Thompson, H. Kazukonis, and J. R. Connell, "750-mm ruling engine producing large gratings and echelles," J. Opt. Soc. Am. **62**, 751–756 (1972).
19. G. R. Harrison, "Techniques for ruling improved large diffraction gratings," Final Report N71-17173 (Massachusetts Institute of Technology, 1971), pp. 1–14.
20. G. R. Harrison and S. W. Thompson, "Large diffraction gratings ruled on a commercial measuring machine controlled interferometrically," J. Opt. Soc. Am. **60**, 591–595 (1970).